Research Article

Lin Chi, Ailian Zhang, Zedong Qiu, Linchun Zhang, Zheng Wang, Shuang Lu*, and Dezhi Zhao

Hydration activity, crystal structural, and electronic properties studies of Ba-doped dicalcium silicate

https://doi.org/10.1515/ntrev-2020-0082
received September 14, 2020; accepted September 30, 2020

Abstract: High belite cement has a wide application potential due to its low energy consumption, low CO_2 emission, and excellent durability performance. Due to the low hydration rate and strength development at an early age, the activation of beta-dicalcium silicate (β-C_2S) crystallographic structure is essential to improve the early strength of high belite cement. In this study, the β-C_2S phase is activated by dissolving Ba^{2+} ions into the crystal lattice to improve the hydration rate. Unlike the traditional analysis methods of thermodynamics and dynamics theory, the first principle and density functional theory were applied to study the effect of Ba^{2+} ions on the activation of β-C_2S, especially on the crystallographic structure, lattice parameters, and electronic structure change. The crystallographic structure of β-C_2S can be activated by doping Ba atom and the crystal formation energy increases and the bandgap between VBM and CBM become narrow in the activated β-C_2S crystallographic structure. Comparing the Ca^{2+} substitution in [CaO_6] or [CaO_8], the lattice deformation and hydraulic reactivity is more significant in Ba_2-C_2S and Ba_{22}-C_2S. The first principle and density functional theory explains the change of the electronic structure of the activated crystallographic structure and provides a theoretical basis for the purposeful design of material structures.

Keywords: crystallographic structural, electronic properties, dicalcium silicate

Highlights

1. The electron structure variation is related to the variation of charge exchange and atomic hybridization orbital in Ba-doped β-C_2S.
2. The lattice deformation and hydraulic reactivity are more significant in Ba-doped β-C_2S with Ba → Ca/[CaO_8].
3. The crystal formation energy increases and the band gap between VBM and CBM become narrow in Ba-doped β-C_2S.

1 Introduction

The traditional cement manufacture has been lasting for less than 200 years. Due to the consumption of high-grade limestones, the high-grade limestone resource in our country is not enough for the next 40 years [1,2]. Therefore, low-grade ore should be used in cement manufacture in point of view of sustainable development. High belite cement has a wide application potential due to its low energy consumption, low CO_2 emission, and excellent durability performance [3–8]. Compared with Ordinary Portland cement, high belite cement consists of more than 40% dicalcium silicate (C_2S) [9,10]. Due to its low CaO consumption, the cement calcining process becomes more energy-saving and a large sum of low-grade ore can be recycled [11–13].

β-C_2S belongs to an island structure, due to the lack of coplanar structure in the $[CaO_x]^{2x-2}$ polyhedron, the length of the Ca^{2+} ion migration path is quite long, thus inhibits the hydraulic reaction of β-C_2S during the hydration process [14,15]. Due to the low hydration rate and strength development in an early age, the application of high-belite cement is limited. The activation of the C_2S

* **Corresponding author: Shuang Lu,** School of Civil Engineering, Harbin Institute of Technology, Harbin 150090, China; Lab of Structures Dynamic Behavior and Control of the Ministry of Education, Harbin Institute of Technology, Harbin 150090, China; Key Lab of Smart Prevention and Mitigation of Civil Engineering Disasters of the Ministry of Industry and Information Technology, Harbin Institute of Technology, Harbin 150090, China, e-mail: hitlu@126.com, tel: +86-13214600050
Lin Chi: School of Environment and Architecture, University of Shanghai for Science and Technology, Shanghai 200093, China
Ailian Zhang, Linchun Zhang: School of Civil Engineering, Sichuan College of Architectural Technology, Deyang, Sichuan 618000, China
Zedong Qiu, Zheng Wang, Dezhi Zhao: School of Civil Engineering, Harbin Institute of Technology, 66 West Dazhi Street, Nangang District, Harbin, 150001, China

crystallographic structure is essential to improve the early strength of high belite cement. By calcining at high temperature, dopant ions are incorporated in the crystal lattice of β-C_2S in the form of the lattice vacancy or site substitution [16,17]. With the reduction of the crystal symmetry and the formation of crystal lattice distortion, the microstress in the lattice increases and the lattice activation of β-C_2S is achieved. Activators such as As_2O_5, V_2O_5, Cr_2O_3, MgO, BaO, CrO, P_2O_5, R_2O, etc. are commonly used in cement industry production [18,19]. At the same time, the addition of activators can effectively reduce the formation energy in chemical reaction thermodynamics [3].

Many researches have studied the activation mechanism of doped ions on the crystal structure transformation of β-C_2S [16,20–23]. Cuesta et al. [24] studied the activation mechanism of doped B^{3+} ions on belite cement and found that Ca^{2+} ions and Si^{4+} ions in the [SiO_4] tetrahedron have been replaced, which contributes to the hydraulic reaction during cement hydration. Wang et al. [25] studied the activation effect of $BaSO_4$ on β-C_2S in belite cement clinker during calcination, and the results showed that $BaSO_4$ could dissolve into the crystal structure of β-C_2S and improve the early compressive strength.

The first principle and density functional theory can explain the change of the electronic structure of the activated crystal structure and also provide a theoretical basis for the purposeful design of the material structure [26–28]. Based on the traditional thermodynamics and kinetics theory, first-principles quantum mechanics calculations have been applied to study the relationship between electronic structure and reaction activity of C_2S polymorphs [29,30]. In this study, the β-C_2S phase is activated by dissolving ions into the crystal lattice to improve the hydration rate. The first principle and density functional theory were applied to study the effect of different ions on the activation of C_2S, especially on the crystallographic structure and lattice parameters and electronic structure change.

2 Materials and methods

2.1 Synthesis of Ba-doped C_2S

Analytical reagents and deionized water are applied during the solution preparation. β-C_2S is synthesized according to ref. [16]. Analytical SiO_2 and CaO with a stoichiometric proportion of Ca:Si = 2:1, 4% $BaSO_4$ with total mass were mixed and ground uniformly by a small ball mill for 20 min until the sieve residue is less than 5%. After mixing anhydrous ethanol, the samples were made into a pill with a diameter of 15 mm and dried in a vacuum drying oven at 105°C. The samples were calcined in the furnace with the calcination temperature 1250°C, the heating rate 10°C/min, and heat preservation for 3 h. The samples were rapid cooling in the case of crystal transformation. The clinker was crushed and ground into a fine powder, and the chemical composition of β-C_2S was analyzed by X-ray fluorescence spectrometry (ThermoFisher, ESCALAB 250Xi).

2.2 Characterization method

The structural variation of β-C_2S doping Ba^{2+} ions was further analyzed by Nuclear Magnetic Resonance (^{29}Si MAS-NMR) and Fourier transform infrared (FT-IR) spectroscopy. ^{29}Si MAS-NMR was measured by a Bruker Avance II 400 MHz spectrometer with a field strength of 9.4 T, operating at 99.2 MHz. The chemical shifts were referenced to tetramethylsilane (TMS). FT-IR patterns were obtained by a Fourier transform infrared spectrometer (Nicolet is5003) with a wave length range from 250 to 4,000 cm^{-1}.

2.3 Molecular dynamics simulation

In this paper, the first principle calculation is based on the density functional theory (DFT) and the plane-wave pseudopotential method (PWP) [31], and the CASTEP module of molecular structure and mechanics simulation software Materials Studio@ (Accelrys 6.2) is employed to calculate the electronic structure and cohesive energy β-C_2S with/without doping Ba ions.

The state of the electronic structure is described by density functional and the generalized gradient approximation (GGA) [32]. The exchange–correlation functionals were calculated using Generalized Gradient Approximation (GGA) with the Perdew–Burke–Ernzerhof functional (PBE functional) [33]. The Brillouin zone was sampled with 4 × 4 × 4 *k*-points in the primitive cell. The values of kinetic energy cutoff E_c and the *k*-points number are increased until the calculated energy converges within the required tolerance, where E_c determines the number of plane waves and *k* points does the sampling of the irreducible wedge of the Brillouin zone [34]. The cutoff energy of plane-wave (PW) was 380 eV,

the energy tolerance was 5×10^{-7} eV/atom, the force tolerance was 0.03 eV/Å, the stress tolerance was 0.05 GPa, and the displacement tolerance was 0.001 Å.

3 Results and analysis

3.1 Activation of Ba-doped β-C_2S

The chemical composition of the calcined Ba-doped C_2S is shown in Table 1, which shows that 2.55% Ba^{2+} is stabilized in the system. The NMR spectrum can reflect the atomic coordination and adjacent atomic effect. The crystallographic structure variation of C_2S reported can be described by the shift of ^{29}Si NMR spectrum [35,36]. Figure 1 shows ^{29}Si spectrum peak shifts and the appearance of the secondary peak right beside the main peak in the NMR spectrum. It infers to the atom subordination change and octahedral transformation in the Ba-doped C_2S.

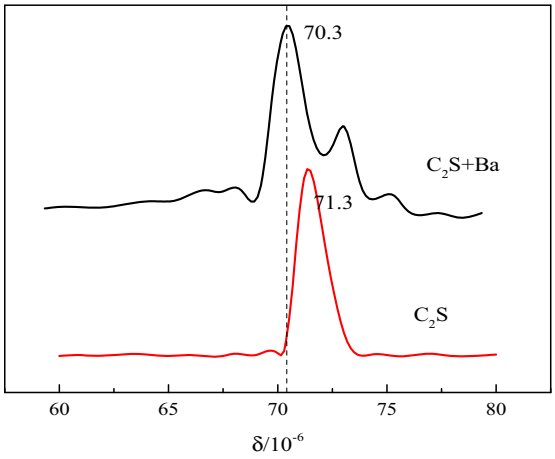

Figure 1: ^{29}Si NMR patterns of β-C_2S phases.

FI-IR analysis was further carried out to verify the lattice variation in Ba-doped C_2S. FT-IR patterns of hydrated β-C_2S and Ba-doped β-C_2S at different curing age are shown in Figure 2. New peaks at 900 and 845 cm^{-1} in Ba-doped β-C_2S are ascribed to the asymmetric stretching vibration of the [SiO_4] tetrahedron, which confirmed that Ba^{2+} enters the crystal lattice after calcination and is consisted with the observation in NMR analysis [37]. The [SiO_4] tetrahedral stretching vibration at 3,440, 1,420, and 1,020 cm^{-1} can be attributed to the formation of C–S–H gel [38]. The appearance of a stronger absorption at 1420 cm^{-1} is attributed to the faster β-C_2S hydration rate after the Ba doping. It can be concluded that Ba^{2+} doping can significantly promote the β-C_2S hydration at an early age.

3.2 Crystal structure and lattice parameters

The lattice parameters of β-C_2S are a = 5.502 Å, b = 6.745 Å, c = 9.297 Å, $\alpha = \gamma = 90.00°$, and $\beta = 94.59°$, which belongs to the monoclinic system with the $P2_1/n_1$ space group [39]. There are 8Ca atoms, 4Si atoms, and 16O atoms in a single Ca_2SiO_4 lattice. According to the lattice model present in Figure 3 by Crystal Maker@ software, Ca atoms can combine with O atom to form [CaO_6] octahedron and [CaO_8] hexahedron. With Ba substituted Ca in β-C_2S lattice, a new solid/solution $Ca_{1-x}Ba_xSiO_4$ (x corresponds to the weight percentage) is formed [15]. Two solid/solution ratios of doped Ba are investigated, $Ca_{1.969}Ba_{0.031}SiO_4$ with single Ba substitution and $Ca_{1.938}Ba_{0.062}SiO_4$ with double Ba substitution [40]. Therefore, $Ba_{1(2)}$-C_2S and $Ba_{11(12,22)}$-C_2S in Table 2 represent two substitution sites of Ca atoms, where Ba_1 and Ba_2 represent Ca atom in the [CaO_6] octahedron and the [CaO_8] hexahedron, respectively. According to the lattice parameters listed in Table 1, the calculated parameters (a = 5.57 Å, b = 6.81 Å, c = 9.37 Å, $\alpha = \gamma = 90.00°$, $\beta = 94.66°$) are basically the same as the theoretical parameters. The error is less than 2%, which confirms the accuracy of the model [41].

When compared with general β-C_2S, the addition of Ba leads to the lattice deformation and the reduction of formation energy in Ba-doped C_2S. The spacing of each crystal plane is increased, and the inner holes are enlarged accordingly. Higher degrees of Ba^{2+} substitution leads to higher variants of crystalline structure. Comparing the Ca^{2+} substitution in [CaO_6] or [CaO_8], the lattice deformation and hydraulic reactivity are more significant in Ba_2-C_2S and Ba_{22}-C_2S.

Table 1: Chemical composition of Ba-doped C_2S (wt%)

Al_2O_3	CaO	SiO_2	Fe_2O_3	K_2O	MgO	P_2O_5	SO_3	BaO	LOI
1.89	62.12	30.06	1.12	0.23	0.67	0.21	0.45	2.55	0.7

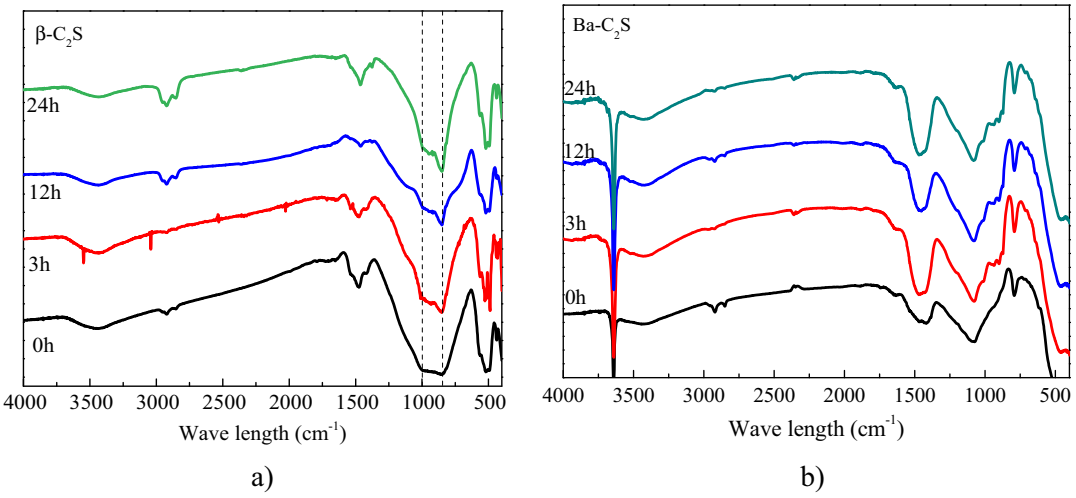

Figure 2: FT-IR patterns of hydrated β-C_2S (left) and Ba-doped β-C_2S (right) at different curing age.

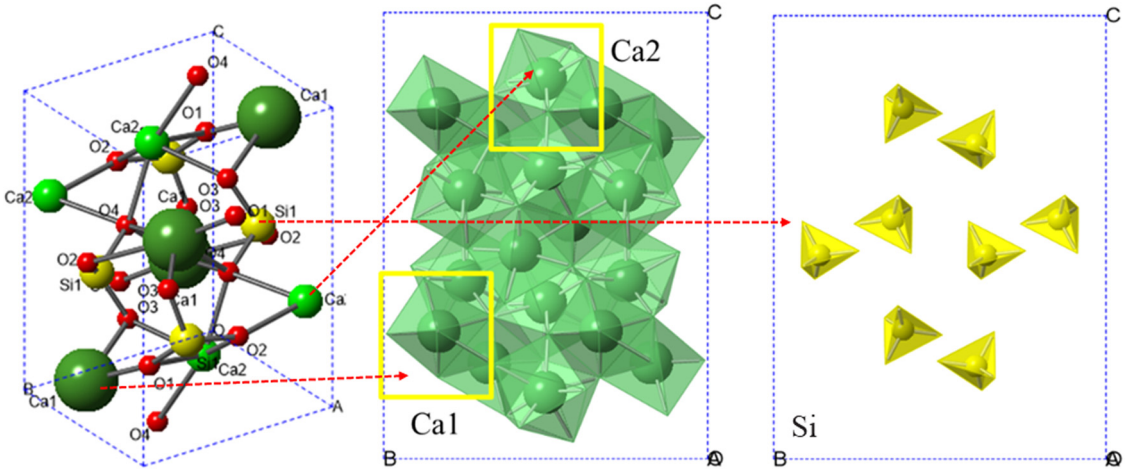

Figure 3: Crystalline structure of β-C_2S (Red balls represent O atoms; green balls represent Ca atoms; yellow balls represent Si atoms.) Ca1 and Ca2 atoms in β-C_2S can combine with O atom to form [CaO_6] octahedron and [CaO_8] hexahedron. Si atom in β-C_2S can combine with O atom to form [SiO_4] tetrahedron.

Table 2: Lattice parameters of β-C_2S and Ba-doped C_2S space group $P2_1/n_1$

	a (Å)	*b* (Å)	*c* (Å)	*α* (°)	*β* (°)	*γ* (°)	Formation energy (eV)
C_2S_{theo} [39]	5.50	6.75	9.30	90	94.59	90	–15480.52
C_2S_{cal}	5.57	6.81	9.37	90	94.66	90	–15481.62
Ba_1-C_2S	5.63	6.99	9.39	90.91	90.93	89.93	–15177.56
Ba_2-C_2S	5.60	6.92	9.63	90.88	93.38	89.55	–15177.47
Ba_{11}-C_2S	5.77	7.09	9.42	91.05	89.22	89.99	–14873.37
Ba_{22}-C_2S	5.67	7.06	9.81	91.36	91.42	89.08	–14873.21
Ba_{12}-C_2S	5.59	7.10	9.71	91.47	92.17	89.66	–14873.29

The low hydraulic reactivity of β-C_2S is ascribed to two aspects, one is the H_2O molecules cannot enter the cavity in the β-C_2S island structure, the other is that Ca attached to the tetrahedron [SiO_4] is not easily dissolved out [28,42]. Pritts et al. [43] have found that Ba, Fe, Al, and Pb doped in β-C_2S clinkers can reduce crystalline symmetry and increase the hydraulic reactivity [40–44]. Due to the limitations of microscopic characterization methods, the correlation between the mechanism of hydration kinetics and the crystallographic structure of Ba-doped C_2S remains to be further studied; therefore, the electronic structure Ba-doped C_2S is further studied in the following.

3.3 Electronic structure of Ba-doped C_2S

The total and partial density of states (TDOS and PDOS) for β-C_2S, $Ba_{1(2)}$-C_2S and $Ba_{11(12,22)}$-C_2S calculated are shown in Figure 4. The main contribution to valence band in β-C_2S

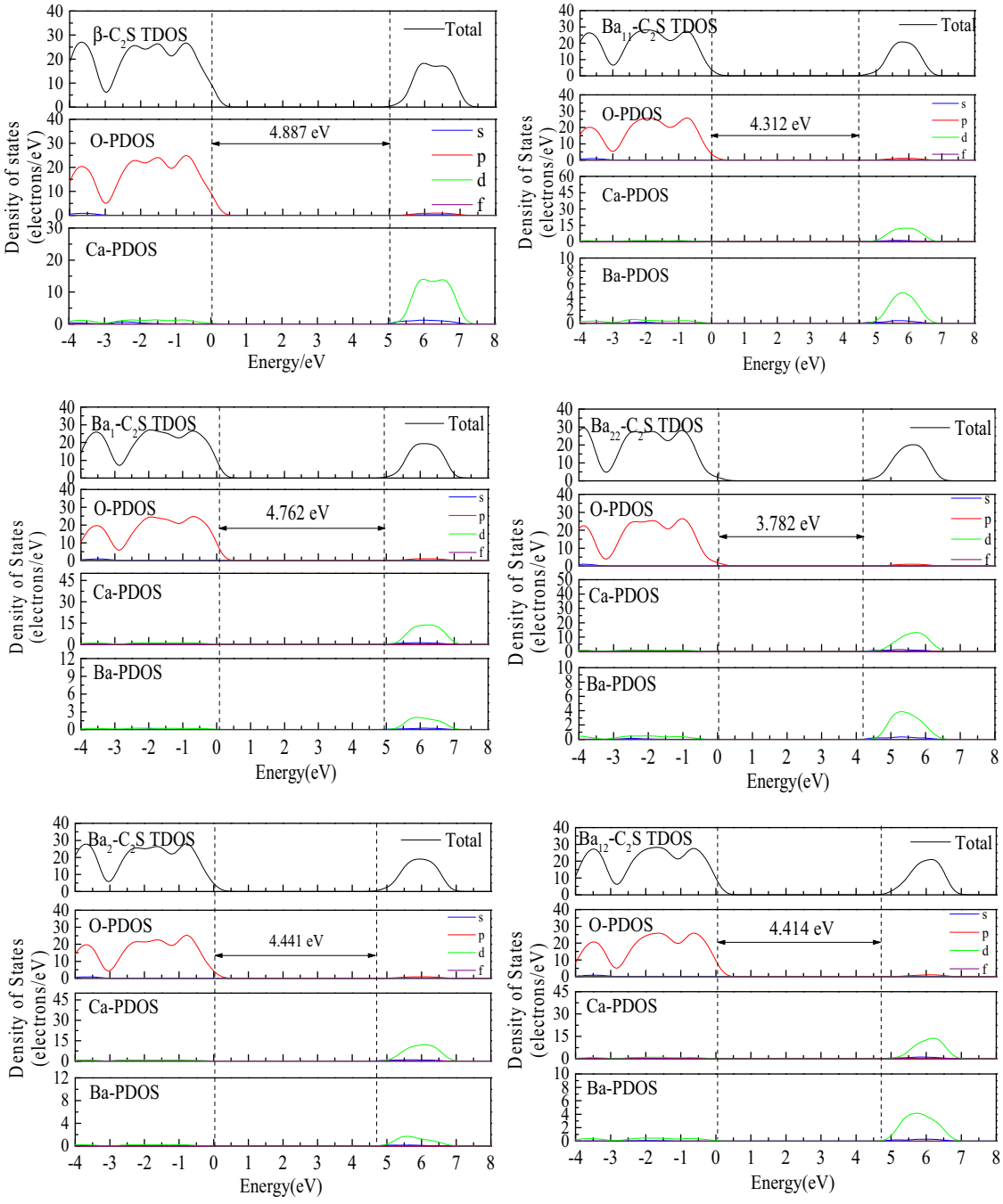

Figure 4: The total and partial density of states (TDOS and PDOS) of β-C_2S and Ba-doped C_2S. Dashed lines represent Fermi energy.

arises from the O-2p located from −4 to 0 eV below the Fermi energy, the main contribution to the conduction band in β-C_2S arises from the Ca-3d located from 5 to 7 eV above the Fermi energy. The band gap between VBM and CBM is 4.887 eV. In the case of $Ba_{1(2)}$-C_2S, the original bond state in the crystal structure has changed with Ba-adopted. Partial contribution to the conduction band comes from the Ba-3d located from 5 to 7 eV. The band gaps in the Ba_1-C_2S and Ba_2-C_2S are 4.762 and 4.441 eV correspondingly. In the case of $Ba_{11(12,22)}$-C_2S, the band gaps between VBM and CBM for each crystal structure are 4.31, 3.78, and 4.41 eV respectively, which indicates that the band gap decreases with the increment of the solid/solution ratios of doped Ba in the system.

According to the coordination theory of crystal chemistry, the cations are filled in the $[CaO_6]$ octahedron when r^{+}/r^{-} = 0.414–0.732; the cations are filled in the $[CaO_8]$ hexahedron when r^{+}/r^{-} = 0.732–1.0. Due to $r_{Ca}{}^{2+}/r_O{}^{2-}$ = 0.75 and $r_{Ba}{}^{2+}/r_O{}^{2-}$ = 1.35/1.32 ≈ 1.0, β-C_2S can incorporate Ba^{2+} by substitution of Ca^{2+} in the $[CaO_8]$ hexahedron instead of $[CaO_6]$ octahedron, with the solid solution of general formula $Ca_{2-x}Ba_xSiO_4$ [37,45]. The formation of coplanar structures of $[Ca(Ba)O_x]^{2x-2}$ polyhedra leads to the structures of the coplanar polyhedron change from spiral chains to three-dimensional network structures [46]. It is suggested that the hydraulic activity of Ba-doped β-C_2S is greatly improved with the formation of Ba–O–Si chains instead of Ca–O–Si chains. When β-C_2S contact with water, the $Ca^{2+}/[CaO_x]^{2x-2}$ polyhedra is dissolved, where OH^- and Si-OH are formed accordingly [40]. Due to the internal forces in the $[CaO_x]^{2x-2}$ are unbalanced, a component force points to the location with Ca^{2+} extracted, which accelerates the continuous dissolution of Ca^{2+} ions. In conclusion, the electron structure variation is related to the variation of charge exchange and atomic hybridization orbital in Ba-doped β-C_2S with different doping positions.

4 Conclusions

The following conclusions can be drawn based on the laboratory investigations:

1. Doping Ba^{2+} in β-C_2S can significantly promote the early hydration. According to the electronic structure and hydraulic reactivity results, the electron structure variation is related to the variation of charge exchange and atomic hybridization orbital in Ba-doped β-C_2S with different doping positions.
2. The hydration kinetics and electronic structure of β-C_2S can be established systematically and intuitively by the first principle calculation. Comparing the Ca^{2+} substitution in $[CaO_6]$ or $[CaO_8]$, the lattice deformation and hydraulic reactivity is more significant in Ba_2-C_2S and Ba_{22}-C_2S.
3. The crystallographic structure of β-C_2S can be activated by doping Ba atom and the crystal formation energy increases and the band gap between VBM and CBM become narrow in the activated β-C_2S crystallographic structure.

Acknowledgments: The authors would like to appreciate the financial sponsored by Shanghai Sailing Program No. 20YF1431800 and National Natural Science Foundation of China (No.51872064).

Author contributions: Investigation, writing – original draft preparation, visualization, software: L. C.; Investigation, formal analysis: A. Z., L. C., D. Z.; Writing – review & editing: S. L., Z. Q.; Supervision: Z. W.

Conflict of interest: The authors declare no conflict of interest regarding the publication of this paper.

References

[1] Benhelal E, Zahedi G, Shamsaei E, Bahadori A. Global strategies and potentials to curb CO_2 emissions in cement industry. J Clean Prod. 2013;51:142–61.
[2] Skalamprinos S, Jen G, Galan I, Whittaker M, Elhoweris A, Glasser F. The synthesis and hydration of ternesite, $Ca_5(SiO_4)_2SO_4$. Cement Concrete Res. 2018;113:27–40.
[3] Stanek T, Sulovsky P. Active low-energy belite cement. Cement. Concrete. Res. 2015;68:203–10.
[4] Huang Y, Qian J, Kang X, Yu J, Fan Y, Dang Y, et al. Belite-calcium sulfoaluminate cement prepared with phospho-gypsum: Influence of P_2O_5 and F on the clinker formation and cement performances. Constr Build Mater. 2019;203:432–42.
[5] Liu Y, Jia M, Song C, Lu S, Wang H, Zhang G, et al. Enhancing ultra-early strength of sulphoaluminate cement-based materials by incorporating graphene oxide. Nanotechnol Rev. 2020;9:1.
[6] Da Costa EB, Rodríguez ED, Bernal SA, Provis JL, Gobbo LA, Kirchheim AP. Production and hydration of calcium sulfoaluminate-belite cements derived from aluminium anodising sludge. Constr Build Mater. 2016;122:373–83.
[7] Meng T, Zhang J, Wei D, Shen J. Effect of nano-strengthening on the properties and microstructure of recycled concrete. Nanotechnol Rev. 2020;9:1.
[8] Zhuang C, Chen Y. The effect of nano-SiO_2 on concrete properties: A review. Nanotechnol Rev. 2019;8(1):562–72.
[9] Rungchet A, Chindaprasirt P, Wansom S, Pimraksa K. Hydrothermal synthesis of calcium sulfoaluminate-belite cement from industrial waste materials. J Clean Prod. 2016;115:273–83.

[10] Chi L, Lu S, Yao Y. Damping additives used in cement-matrix composites: A review. Compos Part B. 2019;164(1):26–36.
[11] Piekkari K, Ohenoja K, Isteri V, Tanskanen P, Illikainen M. Immobilization of heavy metals, selenate, and sulfate from a hazardous industrial side stream by using calcium sulfoaluminate-belite cement. J Clean Prod. 2020;258:120560.
[12] Zheng Y, Li Q, Liu Y. Mine tailing as alternative to clay for producing belite cement clinker. Adv Mater Res. 2013;2704–13.
[13] Ávalos-Rendón TL, Chelala EAP, Mendoza Escobedo CJ, Figueroa IA, Lara VH, Palacios-Romero LM. Synthesis of belite cements at low temperature from silica fume and natural commercial zeolite. Mater Sci Eng. 2018;229:79–85.
[14] Chi L, Wang Z, Lu S, Zhao DZ, Yao Y. Development of mathematical models for predicting the compressive strength and hydration process using the EIS impedance of cementitious materials. Constr Build Mater. 2019;208:652–68.
[15] Qi C, Spagnoli D, Fourie A. DFT-D study of single water adsorption on low-index surfaces of calcium silicate phases in cement. Appl Surf Sci. 2020;518:146255.
[16] Thomas JJ, Ghazizadeh S, Masoero E. Kinetic mechanisms and activation energies for hydration of standard and highly reactive forms of beta-dicalcium silicate (C_2S). Cement Concrete Res. 2017;100:322–28.
[17] Martínez IM, Meseguer-Olmo L, Bernabeu-Esclapez A, Velásquez PA, De Aza PN. In vitro behavior of α-tricalcium phosphate doped with dicalcium silicate in the system Ca_2SiO_4–$Ca_3(PO_4)_2$. Mater Charact. 2012;63:47–55.
[18] Pritts IM, Daugherty KE. The effect of stabilizing agents on the hydration rate of β-C_2S. Cement Concrete Res. 1976;6(6):783–95.
[19] Chen W, Lv G, Hu W, Li D, Chen S, Dai Z. Synthesis and applications of graphene quantum dots: A review. Nanotechnol Rev. 2018;7(2):157–85.
[20] Popescu CD, Muntean M, Sharp JH. Industrial trial production of low energy belite cement. Cement Concrete Comp. 2003;25(7):689–93.
[21] Maiti SC, Ghoroi C. Influence of catalytic nano-additive for stabilization of beta-dicalcium silicate and its hydration rate with different electrolytes. Cement Concrete Res. 2017;98:111–21.
[22] Manohar CS, Kumar BS, Sadhu SPP, Srimadh SK, Varma KBR. Novel Lead-free biocompatible piezoelectric Hydroxyapatite (HA)-BCZT ($Ba_{0.85}Ca_{0.15}Zr_{0.1}Ti_{0.9}O_3$) nanocrystal composites for bone regeneration. Nanotechnol Rev. 2019;8(1):61–78.
[23] Li H, Zhang X, Liu Q, Liu Y, Liu H, Wang X, et al. First-principles calculations of mechanical and thermodynamic properties of tungsten-based alloy. Nanotechnol Rev. 2019;8(1):258–65.
[24] Cuesta A, Losilla ER, Aranda MAG, Sanz J, De la Torre AG. Reactive belite stabilization mechanisms by boron-bearing dopants. Cement Concrete Res. 2012;42(4):598–06.
[25] Wang Z, Ma X, Niu J. Solutionizing of Additional Ions in Belite-rich Clinkers and the Properties of the Resulting Cement. J Wuhan Univ Technol. 2009;24(5):834–37.
[26] Pala MG, Esseni D. Full-band quantum simulation of electron devices with the pseudopotential method: Theory, implementation, and applications. Phys Rev B. 2018;97:12531012.
[27] Sellier JM, Sviercoski RF, Dimov I. On the Wigner Monte Carlo method coupled to pseudopotential models. J Comput Appl Math. 2016;293:217–22.
[28] Wang Q, Li F, Shen X, Shi W, Li X, Guo Y, et al. Relation between reactivity and electronic structure for α′L-, β- and γ-dicalcium silicate: A first-principles study. Cement Concrete Res. 2014;57:28–32.
[29] Durgun E, Manzano H, Pellenq RJM, Grossman JC. Understanding and Controlling the Reactivity of the Calcium Silicate phases from First Principles. Chem Mater. 2012;24(7):1262–67.
[30] Wei L, Cui S, Guo H, Zhang L. The effect of alkali metal over Mn/TiO_2 for low-temperature SCR of NO with NH_3 through DRIFT and DFT. Comp Mater. 2018;144:216–22.
[31] Kuellmer K, Kraemer A, Reith D, Joppich W, Foysi H. Numerical optimisation of the pseudopotential-based lattice Boltzmann method. J Compu Sci. 2016;17:384–93.
[32] Dharmawardhana CC, Misra A, Ching W. Theoretical investigation of C-(A)-S-H(I) cement hydrates. Constr Build Mater. 2018;184:536–48.
[33] Li H, Zhang X, Liu Q, Liu Y, Liu H, Wang X, et al. First-principles calculations of mechanical and thermodynamic properties of tungsten-based alloy. Nanotechnol Rev. 2019;8:258–65.
[34] Shein IR, Ivanovskii AL. Electronic properties of the novel 18-K superconducting Y_2C_3 as compared with 4-K YC_2 from first principles calculations. Solid State Commun. 2004;131(3):223–27.
[35] Schneider J, Cincotto MA, Panepucci H. Si-29 and Al-27 high-resolution NMR characterization of calcium silicate hydrate phases in activated blast-furnace slag pastes. Cement Concrete Res. 2001;31(7):993–01.
[36] Pardal X, Brunet F, Charpentier T, Pochard I, Nonat A. Al-27 and Si-29 Solid-State NMR Characterization of Calcium-Aluminosilicate-Hydrate. Inorg Chem. 2012;51(3):1827–36.
[37] Guan W, Zhao X. Fluoride recovery using porous calcium silicate hydrates via spontaneous Ca2 + and OH− release. Sep Purif Technol. 2016;165:71–7.
[38] Bernard E, Dauzères A, Lothenbach B. Magnesium and calcium silicate hydrates, Part II: Mg-exchange at the interface “low-pH” cement and magnesium environment studied in a C-S-H and M-S-H model system. Appl Geochem. 2018;89:210–18.
[39] Taylor HFW. Cement chemistry. 2nd ed. London: Thomas Telford Publishing; 1990.
[40] Bulina NV, Chaikina MV, Prosanov IY, Dudina DV. Strontium and silicate co-substituted hydroxyapatite: Mechanochemical synthesis and structural characterization. Mater Sci Eng B. 2020;262:114719.
[41] Wang F, Zhang Y, Jiang J, Yin B, Li Z. Effect of temperature on the capillary transport of sodium sulfate solution in calcium silicate hydrate nanopore: A molecular dynamics study. Constr Build Mater. 2020;231:117111.
[42] Azeem M, Azhar Saleem M. Role of electrostatic potential energy in carbon nanotube augmented cement paste matrix. Constr Build Mater. 2020;239:117875.
[43] Pritts IM, Daugherty KE. The effect of stabilizing agents on the hydration rate of β-C2S. Cement Concrete Res. 1976;6(6):783–95.
[44] Zhu G, Li H, Li S, Hou X, Wang X. Crystallization of calcium silicate at elevated temperatures in highly alkaline system of Na_2O-CaO-SiO_2-H_2O. Chinese J Chem Eng. 2017;25(10):1539–44.
[45] Tavakoli D, Tarighat A. Molecular dynamics study on the mechanical properties of Portland cement clinker phases. Comp Mater Sci. 2016;119:65–73.
[46] Zhang X, Zhang Yi, Tian B, Jia Y, Liu Y, Song K, et al. Cr effects on the electrical contact properties of the Al_2O_3-Cu/15W composites. Nanotechnol Rev. 2019;8(1):128–35.